Materials & Design 209 (2021) 109941

Contents lists available at ScienceDirect

Materials & Design

journal homepage: www.elsevier.com/locate/matdes

Enhanced three-dimensional printing scaffold for osteogenesis using a mussel-inspired graphene oxide coating

Ji Min Seok [a,b,1], Goeun Choe [c,1], Sang Jin Lee [a], Min-Ah Yoon [d,e], Kwang-Seop Kim [d,e], Jun Hee Lee [a], Wan Doo Kim [a], Jae Young Lee [c,*,2], Kangwon Lee [b,*,2], Su A Park [a,*,2]

[a] Department of Nature-Inspired System and Application, Korea Institute of Machinery and Materials (KIMM), Daejeon 34103, Republic of Korea
[b] Department of Applied Bioengineering, Graduate School of Convergence Science and Technology, Seoul National University, Seoul 08826, Republic of Korea
[c] School of Materials Science and Engineering, Gwangju Institute of Science and Technology (GIST), Gwangju 61005, Republic of Korea
[d] Department of Nano-Mechatronics, University of Science and Technology (UST), Daejeon 34103, Republic of Korea
[e] Nano-Convergence Manufacturing Systems Research Division, Korea Institute of Machinery and Materials (KIMM), Daejeon 34103, Republic of Korea

HIGHLIGHTS

- Nanomaterial coated scaffolds were fabricated by 3D printing technology.
- The surface of scaffold was modified by controlling the ratio of nanomaterials.
- The bio-inspired scaffolds were shown enhanced osteogenic properties.

GRAPHICAL ABSTRACT

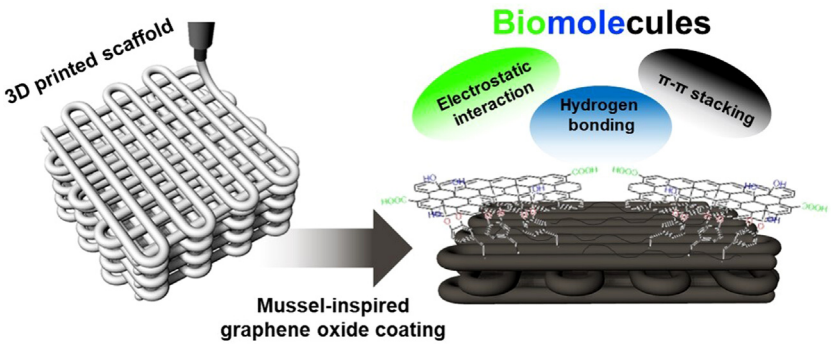

ARTICLE INFO

Article history:
Received 22 January 2021
Revised 27 May 2021
Accepted 27 June 2021
Available online 29 June 2021

Keywords:
3D printing
Bone tissue engineering
Graphene oxide
Polydopamine
Surface modification

ABSTRACT

For further advance a functionality of three-dimensional (3D) printing techniques using biopolymers, graphene oxide (GO) as a carbon-based nanomaterial has received much attention recently due to its superior properties. However, the ability to synergistically affect the resulting 3D-printed structures has been limited by difficulty controlling the nanomaterial ratio in which biological stability is achieved, as well as by the use of noxious solvents applied to the nanomaterials during scaffold fabrication. To address these issues, we demonstrate the use of an ecofriendly mussel-inspired GO coating for 3D-printed scaffolds to enhance the scaffold's functionality and bioactivity. We used polydopamine for deposition using 1, 3, and 6 mg/mL GO in solution on the surface of the scaffold. By this coating method, we efficiently regulated the degree of GO deposition on the surface of scaffold strands under non-toxic conditions, which revealed by microscope. Furthermore, the surface roughness, hydrophilicity, and functional groups were increased after GO coating process. Especially, we identified that the GO coated scaffold was shown improved properties for promoting osteogenesis compared to a bare scaffold by *in vitro* analyses. Therefore, we suggest that the GO coated scaffold has the potential as a bone substitute for tissue engineering.

* Corresponding authors.
E-mail addresses: jaeyouglee@gist.ac.kr (J.Y. Lee), kangwonlee@snu.ac.kr (K. Lee), psa@kimm.re.kr (S.A Park).
[1] These co-authors have made equal contributions to this work.
[2] These corresponding authors have made equal contributions to this work.

https://doi.org/10.1016/j.matdes.2021.109941
0264-1275/

1. Introduction

Considerable advances have been made in the identification of novel natural and synthetic biomaterials for tissue engineering applications that offer the necessary properties of biocompatibility, biodegradability, and nontoxicity in the body [1,2,3]. There has been great interest in nanomaterials for targeted functionality, based on the physical, structural, and chemical properties desired [4,5]. Particularly, carbon-based nanomaterials (CNMs) with various dimensional domains continue to gain attention in the tissue engineering field, due to their excellent mechanical properties for biomedical applications [6,7]. As an example of CNMs, graphene, discovered in 2004, is a single sheet or layered sheet of sp_2-bonded carbon atoms [8]. Graphene derivatives are highly attractive biomaterials for drug delivery [9], engineered liver tissue [10], neural applications [11,12], as well as dental implants [13], due to their unique mechanical, physicochemical, electrical, and biological properties, particularly, biocompatibility [14,15].

Graphene oxide (GO) has been used for bone regeneration, as this material promotes certain cell behaviors and facilitates noncovalent interactions with biomolecules via oxygenated groups on its surfaces [16,17,18,19]. However, with conventional methods, it is difficult to cover large bone defects using only nanomaterials for regeneration, as well as produce customized complex tissue structures. To this end, 3D printing technology can incorporate nanomaterials into biocompatible and biodegradable synthetic polymers to create enhanced scaffold structures for tissue regeneration [20,21,22]. In a recent study by Wang *et al.*, a 3D-printed polycaprolactone (PCL) scaffold incorporating graphene nanosheets showed increased cell proliferation compared to a PCL-only scaffold; the scaffold was easily processable, nontoxic, biocompatible, and biodegradable [23]. Vijayavenkataraman *et al.* created a 3D scaffold using electrohydrodynamic jet 3D printing; the scaffold showed enhanced conductivity and cell differentiation [24]. Despite the ability to customize the scaffold to a particular injury, more extensive injuries tend to require greater amounts of nanomaterials in the composite, potentially introducing negative effects to the body [25]. Moreover, the extrusion printing method has limitations regarding the functionality of the nanomaterial once incorporated into the scaffold strands [26]. Although challenges remain, such as the use of organic solvents in the scaffold coating process that can be potentially toxic to the cells, nanomaterial coating methods provide an alternative for improving the surface functionality of strands making up the scaffold. The development of a stable, nontoxic GO-coating process to enhance the surfaces of 3D-printed tissue scaffolds is necessary for bone tissue regeneration applications.

In this study, a polydopamine (PD) coating, a bioinspired mussel-derived surface modification, was used to establish a nanomaterial coating on the surface of PCL strands of a 3D-printed scaffold for bone tissue regeneration; this surface modification has been extensively used in biomedical applications due to its innocuous effects and strongly adhesive properties in wet conditions [27,28], as well as the ability of the resulting coating to be easily modified for the desired functionality by facilitating the incorporation of various biomolecules and nanomaterials [17,29]. The GO coverage of the strand surfaces is important to the bio-safety of the tissue scaffold. To control the deposition of GO on the surfaces of the strands without toxic methods, we used the PD coating as an intermediate connection between the strand surface and nanomaterial via a dose-dependent process, to ensure biocompatibility and safety.

2. Materials & methods

2.1. Materials

PCL (Mw: 45,000), dopamine hydrochloride, dexamethasone, L-ascorbic acid, and β-glycerophosphate disodium salt hydrate were purchased from Sigma-Aldrich (St. Louis, MO, USA). Dulbecco's Modified Eagle Medium (DMEM, HyClone™, USA) and Minimum Essential Medium Alpha (MEM-α, Gibco, USA) containing 10% fetal bovine serum (FBS; CellSera, Rutherford, Australia) and 1% penicillin/streptomycin (Gibco, USA) were acquired for the cell culture.

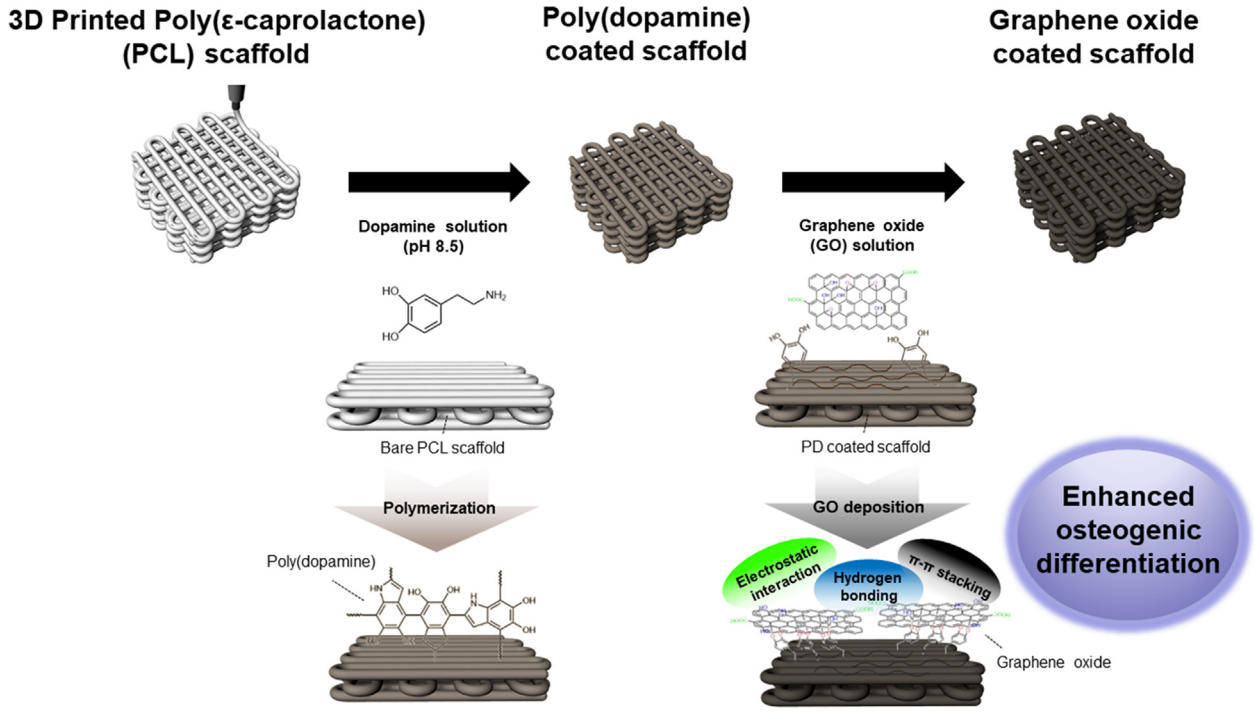

Fig. 1. Schematic diagram of the procedure for the preparation of three-dimensional (3D)-printed polycaprolactone scaffold, polydopamine-coated scaffold, and graphene oxide-coated scaffold.

The GO solution (Graphene Laboratories, Inc., Calverton, NY, USA) was prepared in distilled water (DW) at various doses of 1, 3, and 6 mg/mL GO, respectively. All other reagents were commercially supplied and were of analytical grade.

2.2. Fabrication of GO coated scaffold

The 3D-printed PCL scaffolds were prepared by a laboratory-made system in the Korea Institute of Machinery and Materials [30]. Briefly, the instrument consisted of a 3D *x-y-z* linear stage, a heating block, temperature and pressure controllers, and a computer-aided control system. PCL was melted in a syringe mounted in a heating block for printing through a nozzle at 80 °C. Then the melted PCL was printed on a plate to create a predesigned strand of 400 μm and the desired distance between strands. The edge of the scaffold was cut with an experimental knife to match the uniform size for the optical evaluation. After PCL scaffold fabrication, the construct was immersed in a dopamine hydrochloride solution (2 mg/mL in a 10 mM-Tris buffer; pH: 8.5) for 2 h in a 37 °C drying oven with shaking. Then the PD-coated scaffold was washed with 10 mM-Tris buffer to remove residue, followed by rinsing in DW five times and drying on a clean bench. The dried PD-coated scaffold was dipped in a GO solution of various concentrations. All scaffolds were shaken in the drying oven at 37 °C for overnight. After the GO-coating process, the scaffolds were washed as described for the PD-coated scaffold, and then the samples were stored under vacuum conditions at room temperature (Fig. 1).

2.3. Characterization of the scaffolds

The surface morphologies of the scaffolds were observed by scanning electron microscopy (SEM, FEI, Netherlands) using an acceleration voltage of 10 kV after sputter-coating with Pt. To obtain the topology and surface roughness of the scaffold strands, atomic force microscopy (AFM, Park-System, Korea) measurement in non-contact mode was performed, with a scan area of $5 \times 5\ \mu m^2$. Contact angle measurements (FEMTOFAB, Korea) were used to evaluate the hydrophilicity of the scaffold surfaces at room temperature. X-ray photoelectron spectroscopy (XPS; Thermo Electron Manufacturing Ltd., UK) measurements were acquired over a scan range of 0–1300 eV. Raman spectroscopy (NOST, Korea) was used to collect the spectra under a same exposure time with a single 10-second accumulation in a range from 700 cm^{-1} to 3100 cm^{-1}.

2.4. Preparation of the cell-seeded scaffolds

The scaffolds were washed in ethanol several times, followed by rinsing with phosphate buffered saline (PBS, HyClone™, Hyclone Laboratories, USA). Then the washed scaffolds were dried under ultraviolet conditions on a clean bench for several hours. MC3T3-E1 preosteolasts were cultured in DMEM before seeding, which were incubated with 5% CO_2 at 37 °C. Cells were removed from the culture plate and were gently suspended to attain a seeding density of 5×10^5 cells per scaffold. To stabilize the cell attachment, the cell solution was carefully dropped onto the scaffold several times over the course of a few hours. Then the cell-seeded scaffolds were incubated in DMEM at 5% CO_2 and 37 °C for 2 weeks. For the osteoblastic cell culture, the medium was exchanged with MEM-α containing 0.1 μM dexamethasone, 10 μM L-ascorbic acid, and 10 mM β-glycerophosphate disodium salt hydrate. All processes were carried out under aseptic conditions.

2.5. Cell viability and proliferation

A live/dead cell assay kit (Life Technologies Corp., Carlsbad, CA, USA) was used to measure the viability of the cells after being seeded in the scaffolds for 2 weeks. The working reagent was prepared according to the manufacturer's instructions; the reagent consisted of calcein AM and ethidium homodimer-1 (EthD-1) dissolved in PBS. The cultured scaffolds were washed in PBS several times and then incubated in the prepared reagent for 30 min at 5% CO_2 and 37 °C. After incubation, the dyed cells in the scaffold were measured using a fluorescence microscope (Nikon Corp., Tokyo, Japan) to obtain the cell viability and cytotoxicity. SEM was used to monitor the cell attachment morphology over the 2-week period. After 2 weeks, the cell-seeded scaffolds cultured in DMEM were washed using PBS and then fixed in 4% paraformaldehyde (Lugen Sci Co., Ltd., Gyeonggi-do, Korea). The dehydration of the samples was carried out using graded ethanol at room temperature.

The cell proliferation rate of the scaffold was estimated using a WST-1 cell proliferation assay (Takara Bio Inc., Shiga, Japan) over a 14-day period. WST-1 solution was dissolved in DMEM (10 v/v%) as a working solution for scaffold incubation. Before incubation, the scaffolds were washed in PBS and then incubated for 1 h. A microplate reader (Molecular Devices LLC, San Jose, CA, USA) was used to measure the absorbance of the medium by date at 450 nm.

2.6. Evaluation of osteogenic differentiation

The cell-seeded scaffolds were cultured in osteogenic medium for 2 weeks and then analyzed using an alkaline phosphatase (ALP) assay kit (Takara Bio Inc.). The PBS washed samples were transferred to tubes, to which a radioimmunoprecipitation assay buffer (RIPA buffer, Thermo Fisher Scientific, Waltham, MA, USA) was added to obtain a cell lysate. The tubes were frozen at –80 °C and thawed at 0–4 °C. After repeated freeze-thawing, the cell lysate was sonicated for 5 min and centrifuged at 0–4 °C to remove cell debris. Then *para*-nitrophenyl phosphate substrate solution was added at 1:1 ratio to the cell lysis solution in a 96-well plate, according to the manufacturer's instructions. The mixture was incubated for 1 h at 5% CO_2 and 37 °C. The reaction was stopped by adding a stop solution (0.5 N NaOH) to each well. The absorbance was measured at 405 nm using the same micro reader mentioned earlier in Section 2.5. Activated ALP data were normalized to DNA content using a PicoGreen dsDNA assay kit (Molecular Probes, Eugene, OR, USA), following the instructions provided by the manufacturer.

2.7. Evaluation of mineralization

We examined the mineralization of the cells fixed in the scaffolds over a 2-week period. Alizarin red staining solution (40 mM; pH: 4.2) was applied to the mineralized scaffolds over the course of 1 day at 37 °C. After staining, the scaffolds were washed with DW several times to remove the excess stain. Digital microscopy (ViTiny, USA) images were taken of the samples after stain removal. A QuantiChrom Calcium Assay kit (BioAssay Systems, Hayward, CA, USA) was used to assess the deposition rate of calcium in the scaffold, according to the manufacturer's instructions. SEM was used to determine the mineralization of the scaffold; images were obtained using the procedure detailed above.

2.8. Osteogenic gene expression analyses

The osteogenic relevant gene expression levels were evaluated using a quantitative reverse transcription polymerase chain reaction (qRT-PCR); the levels were normalized with glyceraldehyde-

Table 1
Primer sequence for qRT-RCR analyses.

Gene	Forward	Reverse
GAPDH	5′-AAC TTT GGC ATT GTG GAA GG-3′	5′-ACA CAT TGG GGG TAG GAA CA-3′
Runt-related transcription factor 2 (RunX2)	5′- GCC GGG AAT GAT GAG AAC TA-3′	5′-GGA CCG TCC ACT GTC ACT TT-3′
Osteocalcin (OCN)	5′-CTC CTG AGT CTG ACA AAG CCT T-3′	5′-GCT GTG ACA TCC ATT ACT TGC-3′
Osteopontin (OPN)	5′-TCA GGA CAA CGG AAA GGG-3′	5′-GGA ACT TGC TTG ACT ATC GAT CAC-3′

3-phosphate dehydrogenase (GAPDH) and compared according to the week. Total RNA was extracted after preparation of the cell lysate, according to the manufacturer's instructions, using a Relia-Prep™ RNA Miniprep system (Promega Corp., Madison, WI, USA). The synthesis of cDNA was carried using a QuantiNova™ Reverse Transcription Kit (Qiagen Co., Hilden, Germany). After cDNA was synthesized, qRT-PCR was performed with the primers (Applied Biosystems, Foster City, CA, USA) of osteopontin (OPN), osteocalcin (OCN), and runt-related transcription factor 2 (RunX2); the sequences are listed in Table 1. A comparative threshold cycle (Ct) method was carried out to quantify the osteogenic marker expressions using StepOne software (Applied Biosystems).

2.9. Statistical analyses

The experiments in this study were carried out at least three times; values are presented as the mean ± the standard deviation. Statistical analyses using one-way analysis of variance (ANOVA) with Tukey's *post hoc* test were performed using OriginPro 8.6 software (OriginLab Corp., Northampton, MA, USA); p-values < 0.05 were considered statistically significant.

3. Results & discussion

3.1. Characterization of the fabricated scaffolds

In the recent, 3D printing technology has been extensively used to fabricate the scaffold for tissue engineering applications [31,32]. We designed the scaffold according to the shape of the extensively used scaffold using 3D printing technology which can be layered by patterning in a grid pattern [33,34,35]. The 3D-printed PCL scaffolds were fabricated successfully, according to the predesigned model constructed using a lab-made system, as shown in Fig. 2A. Then the scaffolds were coated with GO, as described in Section 2.2. The structure of the scaffold was fabricated for suitable bone tissue engineering application using the 3D printing system. Reproducible scaffolds were fabricated that retained the interconnected pore structure and pore size of 400 μm, as verified after PD and GO-coating processes; an optimized structure is necessary to promote bone healing [36,37,38]. Furthermore, the PCL scaffold was thoroughly coated with PD and then GO, according to the ratio of the GO solution (1, 3, and 6 mg/mL GO in solution), as shown in Fig. 2B. Dopamine was self-polymerized onto the surfaces of PCL strands making up the scaffold to promote adhesion with macromolecules through Michael addition/Schiff base reactions [27,39,40]. The epoxy group in the chemical structure of GO interconnects with hydroxyl groups in the catechol hydroxyl group of PD [41]. Accordingly, the deposition of GO was confirmed by the increased distribution of particles on the strand surfaces of the PD-coated scaffold.

In Fig. 3A and Table 2, the roughness of the scaffold increased with the GO ratio, as well as the PD coating on the PCL surface, in line with SEM imaging results. In addition, the hydrophilicity of the scaffold increased with the PD coating application, as shown in Fig. 3B. The bare PCL scaffold exhibited hydrophobic surface properties, with a water contact angle of 84.55° measured after 1 min and GO coated groups absorbed water (0°) after water was

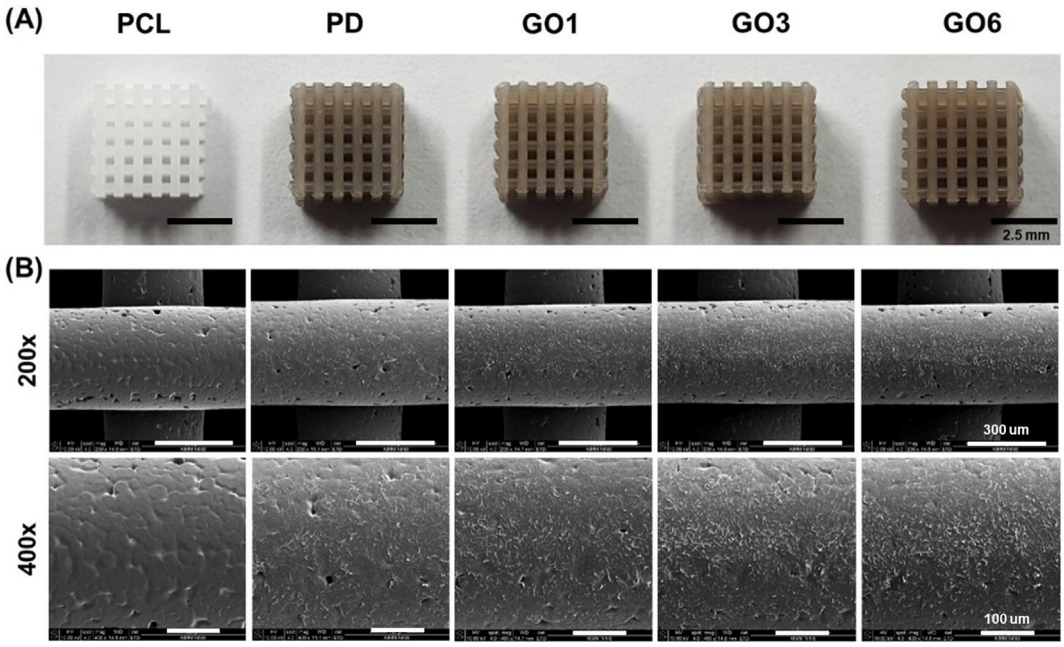

Fig. 2. Fabrication results and surface morphology. (A) Digital camera images of the 3D printed scaffolds (scale bar = 2.5 mm). (B) Scanning electron microscopy (SEM) images of the surface of scaffold strands (scale bar; 200× = 300 μm, 400×= 100 μm). The scaffolds obtained using PCL, PD, GO1, GO3, and GO6 scaffold, respectively (GO1, 3, and 6 containing 1, 3, and 6 mg/mL GO).

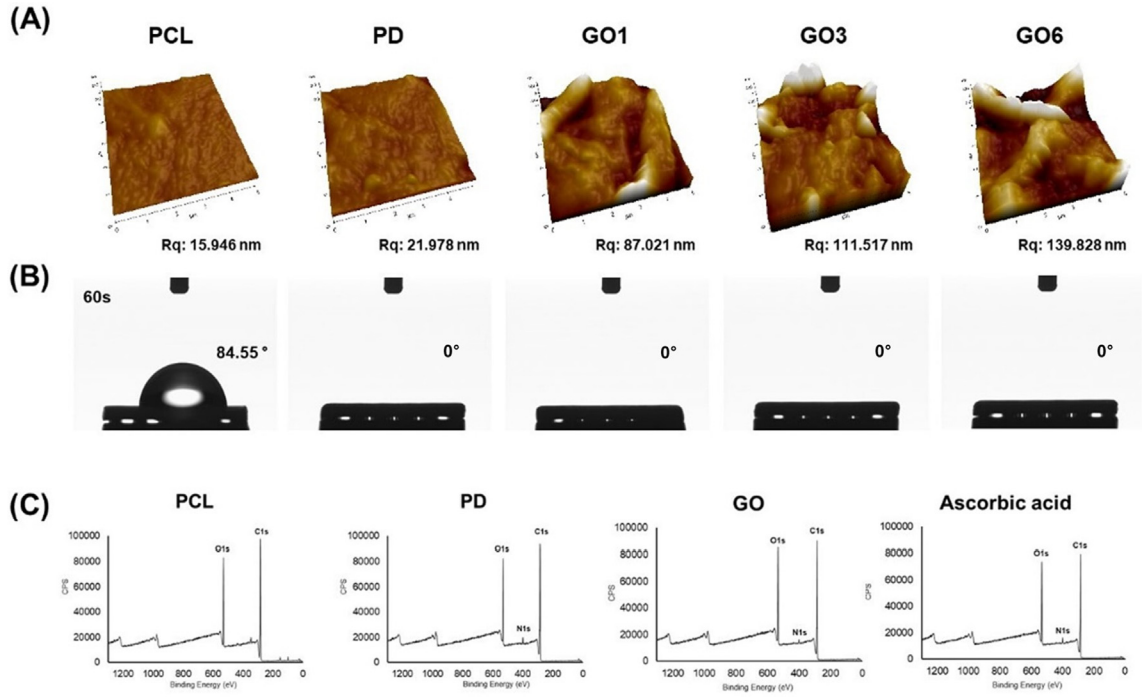

Fig. 3. Surface characterization of strands in the scaffolds. (A) The representative surface image obtained from atomic force microscopy (AFM) using non-contact mode for the scans (Rq: the root mean square of roughness calculated using XEI software [Park-System, Korea]). (B) The contact angle images of the scaffold obtained after 60 s. (C) X-ray photoelectron spectroscopy (XPS) analyses of the scaffolds (PCL: bare PCL scaffold; PD: polydompamine-coated PCL scaffold; GO: graphene oxide-coated PD scaffold; ascorbic acid: GO scaffold with the deposition of the ascorbic acid).

Table 2
X-ray photoelectron spectroscopy elemental percentage of PCL, PD, and GO-coated scaffolds; PCL refers to a bare PCL scaffold; PD refers to a polydompamine-coated PCL scaffold; GO, a graphene oxide-coated PD scaffold using a GO solution with a ratio of 6 mg/mL in distilled water; and an ascorbic acid group indicating a GO scaffold with an ascorbic acid deposition.

	Atomic %			
Elements	PCL	PD	GO	Ascorbic acid
C1s	77.52	75.8	75.16	74.65
N1s	0	2.63	1.63	2.7
O1s	22.48	21.56	23.21	22.65

dropped. In this case, PD formed hydroxyl groups on the PCL surface with hydrophobic $-CH_2$ moieties; in addition, GO has oxygen-containing hydrophilic groups [6,15]. In addition to the hydrophilic modification, the deposition of GO likely facilitates interaction with the biomolecules for bone tissue regeneration [17]. As indicated by the XPS results shown in Fig. 3C, the scaffold successively interacted with the GO material to affect osteogenic differentiation, after deposition onto the surface of the strand in the PD-coated scaffold. The surface of the PD-coated scaffold showed an N 1 s peak that was not present in the PCL group, which has only O 1 s and C 1 s peaks. Particularly, the intensity of the O 1 s peak increased and that of the N 1 s peak decreased after GO deposition, due to oxygen-containing functional epoxide, carboxyl, and hydroxyl groups on the sheet, which are capable of interacting with various osteogenic chemical inducers [42].

To examine the coating degree of the biomolecule as a promoting factor to osteogenic differentiation, the GO-coated scaffold was incubated in 10 μM L-ascorbic acid solution overnight. Our results indicated that the ascorbic acid was incorporated successfully into the GO-coated scaffold, based on the increase in the N 1 s peak. Furthermore, we collected Raman spectra to identify the existence of GO coating on the surface of the strands in the scaffold (Fig. S1). PCL related peaks were measured at 1108 cm^{-1} with C-O-C symmetric stretching, 1446 cm^{-1} with ω(CH2) vibration, 1722 cm^{-1} with ν(C = O) stretching vibration, 2876 and 2920 cm^{-1} with C-H stretching vibration. With polydopamine coating, the peaks at 1330 and 1597 cm^{-1} related with the deformation and stretching of catechol group were shown after polymerization on the PCL surface [43]. Furthermore, the presentative peaks of GO related with D band were shown at 1343 cm^{-1} and G band were shown at 1602 cm^{-1} [44,45]. As demonstrated by these results, the PD coating acts as an intermediary for GO deposition on the PCL scaffold, with full functionality and without the need for an organic solvent. However, it is difficult to control the amount of material delivered to the surface after printing [46,47]. Our ecofriendly coating method efficiently regulated the degree of GO deposition on the surfaces of scaffold strands under nontoxic conditions. Therefore, we anticipate that the biomolecules in the osteoblastic cell culture medium responsible for inducing osteogenic differentiation interact at the scaffold surface via hydrogen bonding with –OH moieties in the substances, π-π stacking between aromatic rings in GO, and through electrostatic repulsion from phosphate ions [9,15,18]. Based on these results, we investigated the performance of our GO-coated scaffolds via *in vitro* tests for bone tissue engineering applications.

3.2. Evaluation of cultured cell viability and proliferation in the scaffolds

After scaffold preparation, we carried out an assessment of the cell viability of osteoblast-like cells after seeding in the scaffolds. The fluorescence intensity from cells grown for 14 days was observed at the point of the cross-sectioned top view in the scaffolds, as shown in Fig. 4A. The signal of the live cells was significant throughout all experimental groups compared to that of dead cells,

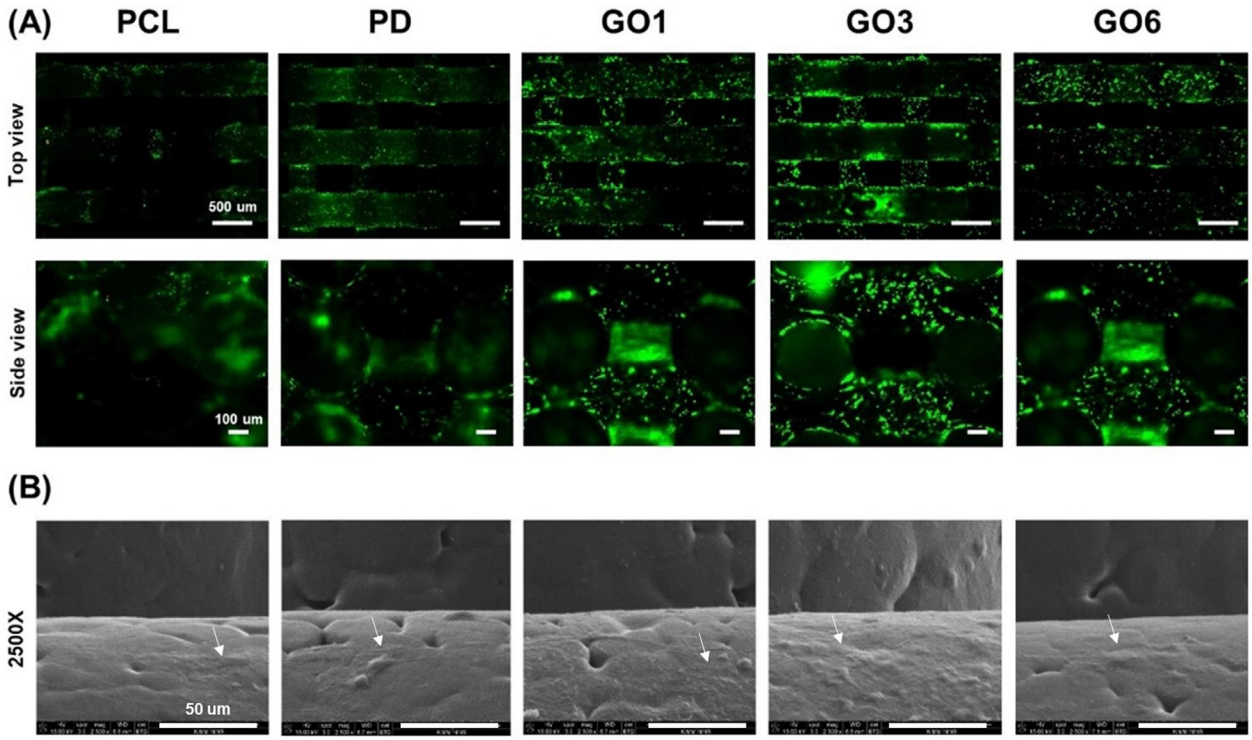

Fig. 4. Viability of cells cultured in the scaffolds. (A) Live/dead assay results of the cultured cells. (B) SEM images of the morphology of the cultured cells on the surfaces of the strands; white arrow. The results were obtained at 14 days (scale bar = 50 μm).

which mainly consisted of PCL; notably, PCL has been approved by the Food and Drug Administration for biomedical application, due to its biocompatible and nontoxic properties [48]. In addition, the PD coating likely promotes the extension of lamellipodia and filopodia of cells for spreading over surfaces [49]. In the case of the GO scaffold, more live dyed cells were evident on the scaffold strands, compared to those of PCL or PD-coated scaffolds. Fig. 4B shows an SEM image of the scaffold surface obtained on Day 14; the cell growth was more dense for the GO scaffolds; this is attributable to the surface modification of the scaffold with GO, which assumes hydrophilic properties. The hydrophilic GO surface enhances cell attachment with spreading [17]. Furthermore, the functional group in GO takes up proteins in the culture medium, which facilitates cell adhesion as well as growth [50,51].

We examined the metabolic activity of cells using a WST-1 assay over a 2-week period; the results are shown in Fig. 5A. Compared to the bare PCL scaffold, the metabolic activity was higher in the PD to GO6 groups at all time points. These results indicate that PD and GO coatings enhance cell growth and biocompatibility. Interestingly, the GO3 group showed distinguishable cell activity compared to the other groups. The PD coating has been shown to reduce the toxicity of the nanomaterial and enhances GO delivery in low concentrations to facilitate tissue regeneration [52]. The scaffold samples showed good cell viability and cytotoxicity, even

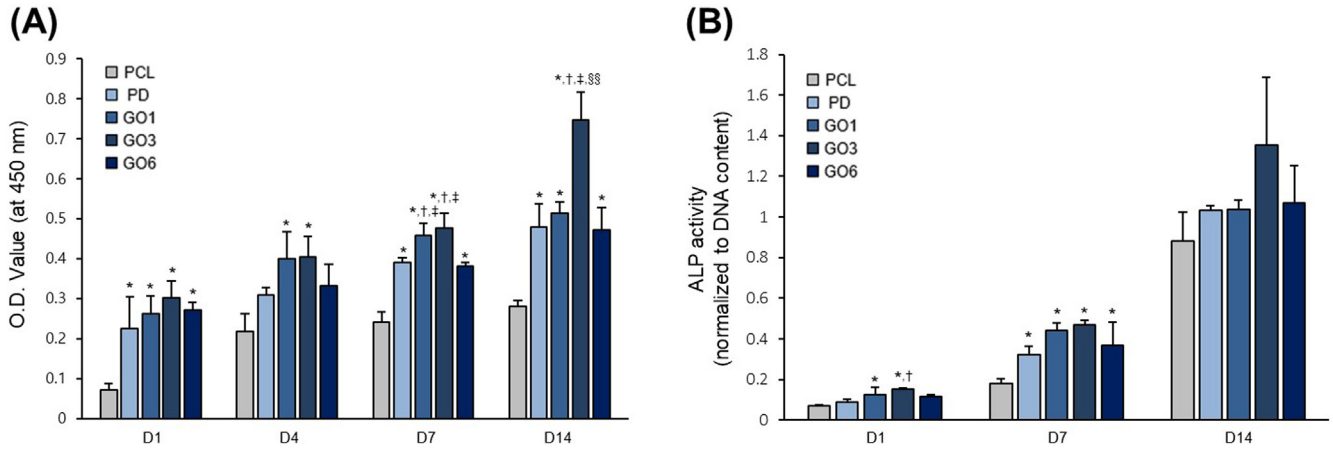

Fig. 5. Proliferation and differentiation of cultured cells in the scaffolds. (A) Results obtained in WST-1 assays. (B) Quantitative analyses of alkaline phosphatase (ALP) activity of the cultured cells; the results were obtained over a 2-week period (n = 3; *compared to PCL, †compared to PD, ‡compared to GO1, and §§compared to GO6 with a significant level of *p < 0.05).

after the coating processes. Based on these results, we examined the osteogenesis of the GO-coated scaffolds.

3.3. Evaluation of osteogenic effects of the scaffolds

To assess the osteogenic differentiation of cells cultured in the scaffolds, we carried out an ALP assay for 2 weeks. Bone-type ALP, an enzyme known to promote hard tissue formation, was used as the osteogenesis marker; additionally, this enzyme is capable of binding to the osteoblast membrane [53]. Fig. 5B shows that the GO-coated scaffold has higher ALP activity than those with PCL only or those coated with PD. This result suggests that the GO-coated scaffold enhances the mineralization process and potentially influences the calcification process [54,55]. Particularly, the ALP activity of the GO3 group increased significantly after 14 days. Thus, control over the ratio of GO on the surface of the scaffold is important to osteogenic differentiation. Based on these results, we anticipate that GO may also enhance mineralization in the cultured cells from the scaffold.

To evaluate the degree of mineralization, we performed alizarin red staining and obtained SEM images of the cultured scaffold with osteoblast-like cells after 14 days. The PCL and PD-coated groups showed a relatively light red color regarding staining of the scaffold strands, as shown in Fig. 6A. On the other hand, the GO-coated scaffolds exhibited a deeper red color than the PCL and PD scaffolds; in particular, the GO3 group was dark red. SEM analyses were conducted to examine the scaffold strand surfaces more closely, as shown in Fig. 6B; mineralized cells appeared on the cultured scaffold in the differentiation medium, with similar characteristics as those reported in previous studies [56,57]. As expected, the GO3 group displayed a greater density of mineralized cells on the surfaces of the scaffold strands. This result suggests that the regulation of the GO ratio affects the cellular deposition of calcium phosphate in the scaffold, which appears to be related to increased ALP activity. We also measured the relative degree of calcium deposition on the cultured scaffold for quantitative evaluation of the level of calcium mineral. As shown in Fig. 6C, the calcium contents of the scaffold increased with the GO deposition on the scaffold following 7 and 14 days, compared to the contents shown on PCL and PD-coated scaffolds. Thus, GO improved the bioactivity of the scaffold, created using an ecofriendly intermediate PD coating on PCL strands and optimized level regarding GO content. As the support materials for the osteogenic differentiation and mineralization of osteoblasts, we speculated that dexamethasone and β-glycerophosphate effectively bind to the surface of the GO scaffold through π-π stacking between aromatic rings [58]. Furthermore, it has been shown that ascorbic acid dissolved in the medium is sufficiently absorbed by hydrogen bonding on the GO dimension to promote osteogenic differentiation [59]. Interestingly, the GO3 group showed exceptional performance, compared to other scaffold types in terms of osteogenic differentiation. To further investigate the effects of GO, we confirmed the osteogenic-related gene expression level through qRT-PCR analyses.

3.4. Evaluation of osteogenic related gene expression

To further determine the osteogenic differentiation level in the cells cultured from the scaffold, we performed qRT-PCR for 2 weeks under osteogenic conditions. The osteogenic relevant genes chosen were RunX2, OCN, and OPN, which are representative osteogenic markers capable of concomitantly regulating bone formation as well as mineralization [60,61]. As shown in Fig. 7, the normalized overall gene expression levels were increased at 2 weeks compared to their 1-week levels. Particularly, the GO-coated groups showed higher expression levels than the control group

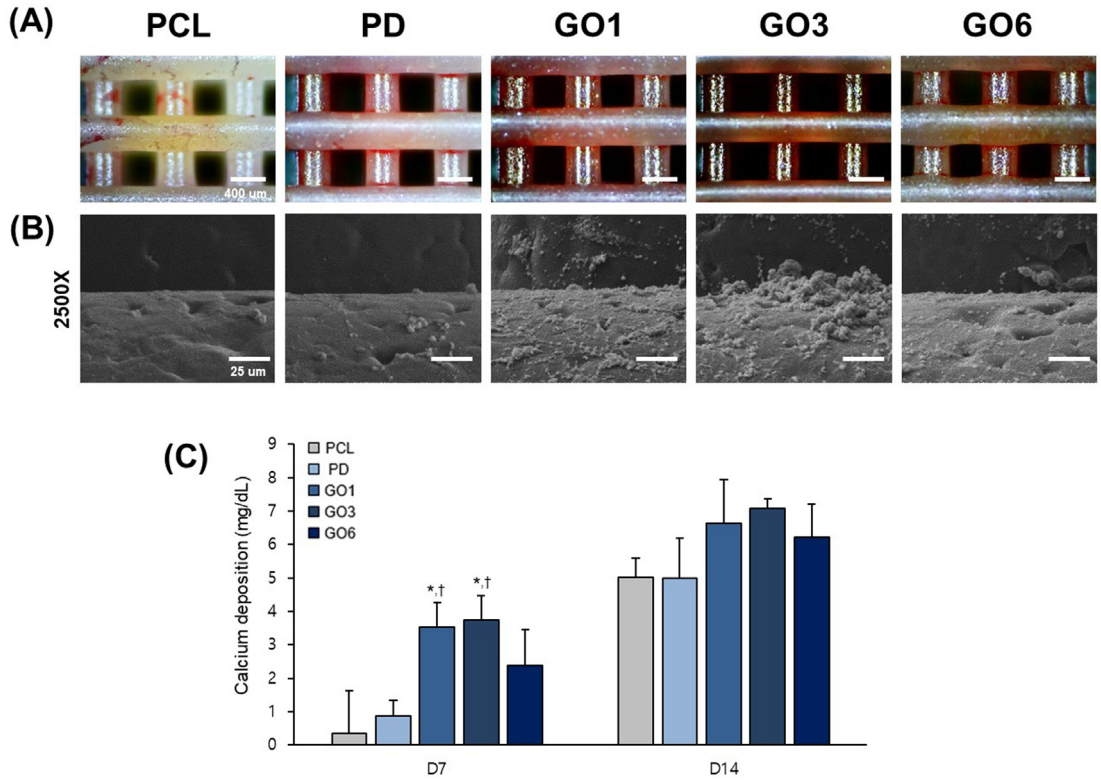

Fig. 6. Osteogenic differentiation and mineralization of the cultured cells in the scaffolds. (A) Alizarin red staining of the cultured scaffold at 14 days (scale bar = 400 μm). (B) SEM images showing the morphology of the mineralized cells on the strand surfaces in the scaffold (scale bar = 50 μm). (C) Quantitative analyses of calcium deposition level of the cultured cells in the scaffolds; the results were obtained over a 2-week period (n = 3; *compared to PCL and †compared to PD for *$p < 0.05$).

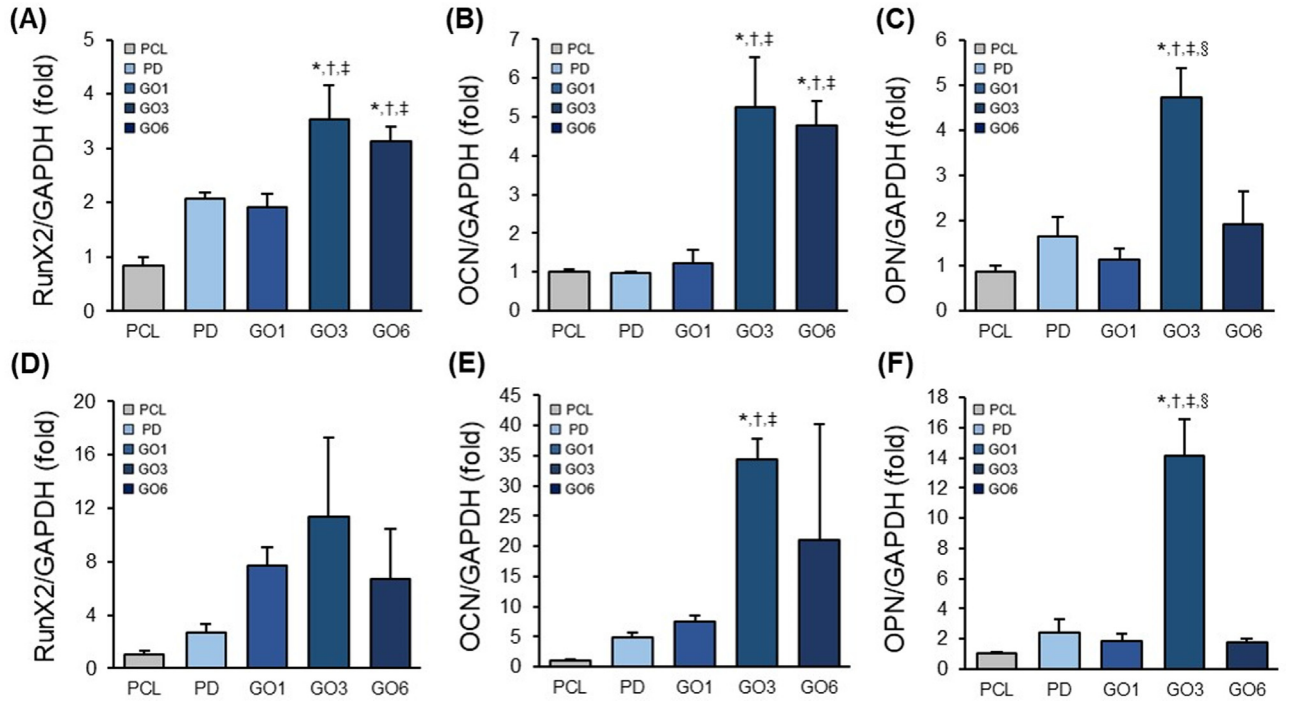

Fig. 7. Osteogenic-related gene expression levels of cultured scaffolds. (A) RunX2, (B) OCN, (C) OPN genes normalized with GAPDH after 1 week. (D) RunX2, (E) OCN, and (F) OPN genes normalized to GAPDH after 2 weeks. (n = 3; *compared to PCL, †compared to PD, ‡compared to GO1, and §compared to GO6 for *p < 0.05).

cultured on the PCL scaffold for 2 weeks. There were no significant differences between the PD and GO1 groups in expression. However, the GO3 group exhibited the highest expression compared to the other scaffold types, indicating that an optimized GO concentration amount (ratio) had been determined. Particularly, the controllable GO-coating process enhanced the surface properties, as well as the bioactivity for osteogenesis and bone regeneration, despite being used in only small amounts for coating the scaffold strand surfaces. We speculate that the biomolecules to support osteogenesis affect the gene expression of cultured cells in the scaffolds, as they are more effectively bound on the GO domain, compared to bare PCL and PD-coated surfaces. Furthermore, these results are consistent with previous results on osteogenic differentiation and mineralization levels of cultured cells in the scaffolds. Therefore, we suggest that our ecofriendly, controllable, GO-coating platform on 3D-printed scaffolds fabricated from biodegradable and biocompatible polymers is promising for TE.

4. Conclusions

A controllable GO-coating platform was presented using an intermediate mussel-inspired PD coating of a bare PCL scaffold. The ecofriendly coating method preserved the functionality of the scaffold. In addition, the scaffold material retained its biosafety/biocompatibility throughout the fabrication process. The coating was successfully regulated according to the ratio of GO and uniform distribution over the strands making up the scaffold. The optimized coating group, GO3, showed significantly enhanced bioactivity compared to the other scaffold types in terms of its ability to promote osteogenesis and therapeutic payload delivery (e.g., drugs, proteins, growth factors, and so forth) due to the various hydrophilic and aromatic moieties of the GO domain. Thus, based on our results, the ecofriendly, mussel-inspired, GO-coated, 3D-printed scaffolds show tremendous potential for bone tissue engineering and biomedical applications.

CRediT authorship contribution statement

Ji Min Seok: Writing - original draft, Conceptualization. **Goeun Choe:** Conceptualization. **Sang Jin Lee:** Methodology, Formal analysis. **Min-Ah Yoon:** Methodology, Formal analysis. **Kwang-Seop Kim:** Methodology, Formal analysis. **Jun Hee Lee:** Methodology, Formal analysis. **Wan Doo Kim:** Investigation, Resources. **Jae Young Lee:** Supervision. **Kangwon Lee:** Supervision. **Su A Park:** Writing - review & editing, Supervision.

Declaration of Competing Interest

The authors declare that they have no known competing financial interests or personal relationships that could have appeared to influence the work reported in this paper.

Acknowledgments

This research was supported by the National Research Foundation (NRF) funded by the Korean government (MSIT; No. NRF-2019M3A9E2066348, 2020M3H4A1A02084828 and 2021M3H4A4079292).

Appendix A. Supplementary material

Supplementary data to this article can be found online at https://doi.org/10.1016/j.matdes.2021.109941.

References

[1] H. Shin, S. Jo, A.G. Mikos, Biomimetic Materials for Tissue Engineering, Biomaterials 24 (2003) 4353–4364, https://doi.org/10.1016/S0142-9612(03)00339-9.

[2] T.H. Qazi, D.J. Mooney, M. Pumberger, S. Geiβler, G.N. Duda, Biomaterials-Based Strategies for Skeletal Muscle Tissue Engineering: Existing Technologies and Future Trends, Biomaterials 53 (2015) 502–521, https://doi.org/10.1016/j.biomaterials.2015.02.110.

[3] A.K. Gaharwar, I. Singh, A. Khademhosseini, Engineered Biomaterials for In Situ Tissue Regeneration, Nat. Rev. Mater. 5 (2020) 686–705, https://doi.org/10.1038/s41578-020-0209-x.
[4] L. Zhang, T.J. Webster, Nanotechnology and Nanomaterials: Promises for Improved Tissue Regeneration, Nano Today 4 (2009) 66–80, https://doi.org/10.1016/j.nantod.2008.10.014.
[5] T. Gong, J. Xie, J. Liao, T. Zhang, S. Lin, Y. Lin, Nanomaterials and Bone Regeneration. Bone Res. 3 (2015) 15029, https://doi.org/10.1038/boneres.2015.29.
[6] C. Cha, S.R. Shin, N. Annabi, M.R. Dokmeci, A. Khademhosseini, Carbon-Based Nanomaterials: Multifunctional Materials for Biomedical Engineering, ACS Nano 7 (2013) 2891–2897, https://doi.org/10.1021/nn401196a.
[7] S.H. Ku, M. Lee, C.B. Park, Carbon-Based Nanomaterials for Tissue Engineering, Adv. Healthcare Mater. 2 (2013) 244–260, https://doi.org/10.1002/adhm.201200307.
[8] K.S. Novoselov, A.K. Geim, S.V. Morozov, D. Jiang, Y. Zhang, S.V. Dubonos, I.V. Grigorieva, A.A. Firsov, Electric Field in Atomically Thin Carbon Films, Science 306 (2004) 666–669, https://doi.org/10.1126/science.1102896.
[9] W.R. Zhuang, Y. Wang, P.F. Cui, L. Xing, J. Lee, D. Kim, H.L. Jiang, Y.K. Oh, Applications of π-π Stacking Interactions in the Design of Drug-Delivery Systems, J. Control. Release 294 (2019) 311–326, https://doi.org/10.1016/j.jconrel.2018.12.014.
[10] R.G. Bai, K. Muthoosamy, S. Manickam, A. Hilal-Alnaqbi, Graphene-Based 3D Scaffolds in Tissue Engineering: Fabrication, Applications, and Future Scope in Liver Tissue Engineering, Int. J. Nanomedicine 14 (2019) 5753–5783, https://doi.org/10.2147/IJN.S192779.
[11] S.Y. Park, J. Park, S.H. Sim, M.G. Sung, K.S. Kim, B.H. Hong, S. Hong, Enhanced Differentiation of Human Neural Stem Cells into Neurons on Graphene, Adv. Mater. 23 (2011) H263–H267, https://doi.org/10.1002/adma.201101503.
[12] O. Akhavan, E. Ghaderi, S.A. Shirazian, R. Rahighi, Rolled graphene oxide foams as three-dimensional scaffolds for growth of neural fibers using electrical stimulation of stem cells, Carbon 97 (2016) 71–77, https://doi.org/10.1016/j.carbon.2015.06.079.
[13] R. Guazzo, C. Gardin, G. Bellin, L. Sbricoli, L. Ferroni, F.S. Ludovichetti, A. Piattelli, I. Antoniac, E. Bressan, B. Zavan, Graphene-Based Nanomaterials for Tissue Engineering in the Dental Field, Nanomaterials 8 (2018) 349, https://doi.org/10.3390/nano8050349.
[14] H. Chen, M.B. Müller, K.J. Gilmore, G.G. Wallace, D. Li, Mechanically Strong, Electrically Conductive, and Biocompatible Graphene Paper, Adv. Mater. 20 (2008) 3557–3561, https://doi.org/10.1002/adma.200800757.
[15] Y. Qu, F. He, C. Yu, X. Liang, D. Liang, L. Ma, Q. Zhang, J. Lv, J. Wu, Advances in Graphene-Based Nanomaterials for Biomedical Applications, Mater. Sci. Eng. C 90 (2018) 764–780, https://doi.org/10.1016/j.msec.2018.05.018.
[16] Z. Peng, T. Zhao, Y. Zhou, S. Li, J. Li, R.M. Leblanc, Bone Tissue Engineering via Carbon-Based Nanomaterials, Adv. Healthcare Mater. 9 (2020) 1901495, https://doi.org/10.1002/adhm.201901495.
[17] X. Cheng, Q. Wan, X. Pei, Graphene Family Materials in Bone Tissue Regeneration: Perspectives and Challenges, Nanoscale Res. Lett. 13 (2018) 289, https://doi.org/10.1186/s11671-018-2694-z.
[18] E. Nishida, H. Miyaji, H. Takita, I. Kanayama, M. Tsuji, T. Akasaka, T. Sugaya, R. Sakagami, M. Kawanami, Graphene Oxide Coating Facilitates the Bioactivity of Scaffold Material for Tissue Engineering, Jpn. J. Appl. Phys. 53 (2014) 06JD04, https://doi.org/10.7567/JJAP.53.06JD04.
[19] O. Akhavan, E. Ghaderi, M. Shahsavar, Graphene nanogrids for selective and fast osteogenic differentiation of human mesenchymal stem cells, Carbon 59 (2013) 200–211, https://doi.org/10.1016/j.carbon.2013.03.010.
[20] M.A. Heinrich, W. Liu, A. Jimenez, J. Yang, A. Akpek, X. Liu, Q. Pi, X. Mu, N. Hu, R. M. Schiffelers, J. Prakash, J. Xie, Y.S. Zhang, 3D Bioprinting: From Benches to Translational Applications, Small 15 (2019) 1805510, https://doi.org/10.1002/smll.201805510.
[21] S.H. Park, C.S. Jung, B.H. Min, Advances in Three-Dimensional Bioprinting for Hard Tissue Engineering, Tissue Eng. Regen. Med. 13 (2016) 622–635, https://doi.org/10.1007/s13770-016-0145-4.
[22] R. Singla, S.M.S. Abidi, A.I. Dar, A. Acharya, Nanomaterials as Potential and Versatile Platform for next Generation Tissue Engineering Applications, J. Biomed. Mater. Res. - Part B Appl. Biomater. 107 (2019) 2433–2449, https://doi.org/10.1002/jbm.b.34327.
[23] W. Wang, G. Caetano, W.S. Ambler, J.J. Blaker, M.A. Frade, P. Mandal, C. Diver, P. Bártolo, Enhancing the Hydrophilicity and Cell Attachment of 3D Printed PCL/graphene Scaffolds for Bone Tissue Engineering, Materials (Basel) 9 (2016) 992, https://doi.org/10.3390/ma9120992.
[24] S. Vijayavenkataraman, S. Thaharah, S. Zhang, W.F. Lu, J.Y.H. Fuh, 3D-Printed PCL/rGO Conductive Scaffolds for Peripheral Nerve Injury Repair, Artif. Organs 43 (2019) 515–523, https://doi.org/10.1111/aor.13360.
[25] K. Wang, J. Ruan, H. Song, J. Zhang, Y. Wo, S. Guo, D. Cui, Biocompatibility of Graphene Oxide, Nanoscale Res. Lett. 6 (2011) 1–8, https://doi.org/10.1007/s11671-010-9751-6.
[26] G.F. Caetano, W. Wang, W.H. Chiang, G. Cooper, C. Diver, J.J. Blaker, M.A. Frade, P. Bártolo, 3D-Printed Poly(ϵ-Caprolactone)/graphene Scaffolds Activated with p1-Latex Protein for Bone Regeneration. 3D Print, Addit. Manuf. 5 (2018) 127–137, https://doi.org/10.1089/3dp.2018.0012.
[27] H. Lee, S.M. Dellatore, W.M. Miller, P.B. Messersmith, Mussel-Inspired Surface Chemistry for Multifunctional Coatings, Science 318 (2007) 426–430, https://doi.org/10.1126/science.1147241.
[28] M. Liu, G. Zeng, K. Wang, Q. Wan, L. Tao, X. Zhang, Y. Wei, Recent Developments in Polydopamine: An Emerging Soft Matter for Surface Modification and Biomedical Applications, Nanoscale 8 (2016) 16819–16840, https://doi.org/10.1039/c5nr09078d.
[29] A. Hermenean, A. Codreanu, H. Herman, C. Balta, M. Rosu, C.V. Mihali, A. Ivan, S. Dinescu, M. Ionita, M. Costache, Chitosan-Graphene Oxide 3D Scaffolds as Promising Tools for Bone Regeneration in Critical-Size Mouse Calvarial Defects, Sci. Rep. 7 (2017) 16641, https://doi.org/10.1038/s41598-017-16599-5.
[30] S.J. Lee, D. Lee, T.R. Yoon, H.K. Kim, H.H. Jo, J.S. Park, J.H. Lee, W.D. Kim, I.K. Kwon, S.A. Park, Surface Modification of 3D-Printed Porous Scaffolds via Mussel-Inspired Polydopamine and Effective Immobilization of rhBMP-2 to Promote Osteogenic Differentiation for Bone Tissue Engineering, Acta Biomater. 40 (2016) 182–191, https://doi.org/10.1016/j.actbio.2016.02.006.
[31] L. Dong, S.J. Wang, X.R. Zhao, Y.F. Zhu, J.K. Yu, 3D-printed poly (ϵ-caprolactone) scaffold integrated with cell-laden chitosan hydrogels for bone tissue engineering, Sci. Rep. 7 (2017) 4–12, https://doi.org/10.1038/s41598-017-13838-7.
[32] Y. She, Z. Fan, L. Wang, Y. Li, W. Sun, H. Tang, L. Zhang, L. Wu, H. Zheng, C. Chen, 3D Printed Biomimetic PCL Scaffold as Framework Interspersed With Collagen for Long Segment Tracheal Replacement, Front. Cell Dev. Biol. 9 (2021) 1–14, https://doi.org/10.3389/fcell.2021.629796.
[33] Z. Jiao, B. Luo, S. Xiang, H. Ma, Y. Yu, W. Yang, 3D printing of HA / PCL composite tissue engineering scaffolds, Adv. Ind. Eng. Polym. Res. 2 (2019) 196–202, https://doi.org/10.1016/j.aiepr.2019.09.003.
[34] G. Li, L. Wang, W. Pan, F. Yang, W. Jiang, X. Wu, X. Kong, K. Dai, Y. Hao, In vitro and in vivo study of additive manufactured porous Ti6Al4V scaffolds for repairing bone defects, Sci. Rep. 6 (2016) 1–11, https://doi.org/10.1038/srep34072.
[35] F.S.L. Bobbert, A.A. Zadpoor, Effects of bone substitute architecture and surface properties on cell response, angiogenesis, and structure of new bone, J. Mater. Chem. B. 5 (2017) 6175–6192, https://doi.org/10.1039/c7tb00741h.
[36] X. Liu, P.X. Ma, Polymeric Scaffolds for Bone Tissue Engineering, Ann. Biomed. Eng. 32 (2004) 477–486, https://doi.org/10.1023/B:ABME.0000017544.36001.8e.
[37] S. Wu, X. Liu, K.W.K. Yeung, C. Liu, X. Yang, Biomimetic Porous Scaffolds for Bone Tissue Engineering, Mater. Sci. Eng. R Reports 80 (2014) 1–36, https://doi.org/10.1016/j.mser.2014.04.001.
[38] K. Rezwan, Q.Z. Chen, J.J. Blaker, A.R. Boccaccini, Biodegradable and Bioactive Porous Polymer/inorganic Composite Scaffolds for Bone Tissue Engineering, Biomaterials 27 (2006) 3413–3431, https://doi.org/10.1016/j.biomaterials.2006.01.039.
[39] J.B. Choi, Y.S. Jang, S. Mi Byeon, J. Hwa Jang, Y.K. Kim, T.S. Bae, M.H. Lee, Effect of Composite Coating with Poly-dopamine/PCL on the Corrosion Resistance of Magnesium, Int. J. Polym. Mater. Polym. Biomater. 68 (2019) 328–337, https://doi.org/10.1080/00914037.2018.1455678.
[40] L. Jia, F. Han, H. Wang, C. Zhu, Q. Guo, J. Li, Z. Zhao, Q. Zhang, X. Zhu, B. Li, Polydopamine-Assisted Surface Modification for Orthopaedic Implants, J. Orthop. Transl. 17 (2019) 82–95, https://doi.org/10.1016/j.jot.2019.04.001.
[41] C. Cheng, S. Nie, S. Li, H. Peng, H. Yang, L. Ma, S. Sun, C. Zhao, Biopolymer Functionalized Reduced Graphene Oxide with Enhanced Biocompatibility via Mussel Inspired Coatings/anchors, J. Mater. Chem. B 1 (2013) 265–275, https://doi.org/10.1039/c2tb00025c.
[42] S.J. Lee, H.J. Lee, S.Y. Kim, J.M. Seok, J.H. Lee, W.D. Kim, I.K. Kwon, S.Y. Park, S.A. Park, In Situ Gold Nanoparticle Growth on Polydopamine-Coated 3D-Printed Scaffolds Improves Osteogenic Differentiation for Bone Tissue Engineering Applications, Vitro and In Vivo Studies. Nanoscale 10 (2018) 15447–15453, https://doi.org/10.1039/c8nr04037k.
[43] Y. Deng, W.Z. Yang, D. Shi, M. Wu, X.L. Xiong, Z.G. Chen, S.C. Wei, Bioinspired and osteopromotive polydopamine nanoparticle-incorporated fibrous membranes for robust bone regeneration, NPG Asia Mater. 11 (2019) 39, https://doi.org/10.1038/s41427-019-0139-5.
[44] M. Cui, S. Ren, H. Zhao, Q. Xue, L. Wang, Polydopamine coated graphene oxide for anticorrosive reinforcement of water-borne epoxy coating, Chem. Eng. J. 335 (2018) 255–266, https://doi.org/10.1016/j.cej.2017.10.172.
[45] O. Akhavan, Bacteriorhodopsin as a superior substitute for hydrazine in chemical reduction of single-layer graphene oxide sheets, Carbon 81 (2015) 158–166, https://doi.org/10.1016/j.carbon.2014.09.044.
[46] G. Turnbull, J. Clarke, F. Picard, P. Riches, L. Jia, F. Han, B. Li, W. Shu, 3D Bioactive Composite Scaffolds for Bone Tissue Engineering, Bioact. Mater. 3 (2018) 278–314, https://doi.org/10.1016/j.bioactmat.2017.10.001.
[47] H. Guo, R. Lv, S. Bai, Recent Advances on 3D Printing Graphene-Based Composites, Nano Mater. Sci. 1 (2019) 101–115, https://doi.org/10.1016/j.nanoms.2019.03.003.
[48] E. Malikmammadov, T.E. Tanir, A. Kiziltay, V. Hasirci, N. Hasirci, PCL and PCL-Based Materials in Biomedical Applications, J. Biomater. Sci. Polym. Ed. 29 (2018) 863–893, https://doi.org/10.1080/09205063.2017.1394711.
[49] X. Gao, J. Song, P. Ji, X. Zhang, X. Li, X. Xu, M. Wang, S. Zhang, Y. Deng, F. Deng, S. Wei, Polydopamine-Templated Hydroxyapatite Reinforced Polycaprolactone Composite Nanofibers with Enhanced Cytocompatibility and Osteogenesis for Bone Tissue Engineering, ACS Appl. Mater. Interfaces 8 (2016) 3499–3515, https://doi.org/10.1021/acsami.5b12413.
[50] C. Zhong, J. Feng, X. Lin, Q. Bao, Continuous Release of Bone Morphogenetic Protein-2 through Nano-Graphene Oxide-Based Delivery Influences the Activation of the NF-κB Signal Transduction Pathway, Int. J. Nanomedicine 12 (2017) 1215–1226, https://doi.org/10.2147/IJN.S124040.
[51] W.G. La, M. Jin, S. Park, H.H. Yoon, G.J. Jeong, S.H. Bhang, H. Park, K. Char, B.S. Kim, Delivery of Bone Morphogenetic Protein-2 and Substance P Using

Graphene Oxide for Bone Regeneration, Int. J. Nanomedicine 9 (2014) 107–116, https://doi.org/10.2147/IJN.S50742.
[52] S. Hong, K.Y. Kim, H.J. Wook, S.Y. Park, K.D. Lee, D.Y. Lee, H. Lee, Attenuation of the In Vivo Toxicity of Biomaterials by Polydopamine Surface Modification, Nanomedicine 6 (2011) 793–801, https://doi.org/10.2217/nnm.11.76.
[53] A. Sengottuvelan, P. Balasubramanian, J. Will, A.R. Boccaccini, Bioactivation of Titanium Dioxide Scaffolds by ALP-Functionalization, Bioact. Mater. 2 (2017) 108–115, https://doi.org/10.1016/j.bioactmat.2017.02.004.
[54] Z. Fan, J. Wang, F. Liu, Y. Nie, L. Ren, B. Liu, A New Composite Scaffold of Bioactive Glass Nanoparticles/graphene: Synchronous Improvements of Cytocompatibility and Mechanical Property, Colloids Surf. B Biointerfaces 145 (2016) 438–446, https://doi.org/10.1016/j.colsurfb.2016.05.026.
[55] H. Elkhenany, L. Amelse, A. Lafont, S. Bourdo, M. Caldwell, N. Neilsen, E. Dervishi, O. Derek, A.S. Biris, D. Anderson, M. Dhar, Graphene Supports In Vitro Proliferation and Osteogenic Differentiation of Goat Adult Mesenchymal Stem Cells: Potential for Bone Tissue Engineering, J. Appl. Toxicol. 35 (2015) 367–374, https://doi.org/10.1002/jat.3024.
[56] M. López-Álvarez, I. Pereiro, J. Serra, A. De Carlos, P. González, Osteoblast-like Cell Response to Macro- and Micro-Patterned Carbon Scaffolds Obtained from the Sea Rush Juncus Maritimus, Biomed. Mater. 6 (2011), https://doi.org/10.1088/1748-6041/6/4/045012 045012.
[57] S.F. Lamolle, M. Monjo, M. Rubert, H.J. Haugen, S.P. Lyngstadaas, J.E. Ellingsen, The Effect of Hydrofluoric Acid Treatment of Titanium Surface on Nanostructural and Chemical Changes and the Growth of MC3T3-E1 Cells, Biomaterials 30 (2009) 736–742, https://doi.org/10.1016/j.biomaterials.2008.10.052.
[58] W.C. Lee, C.H.Y.X. Lim, H. Shi, L.A.L. Tang, Y. Wang, C.T. Lim, K.P. Loh, Origin of Enhanced Stem Cell Growth and Differentiation on Graphene and Graphene Oxide, ACS Nano 5 (2011) 7334–7341, https://doi.org/10.1021/nn202190c.
[59] W. Qi, W. Yuan, J. Yan, H. Wang, Growth and Accelerated Differentiation of Mesenchymal Stem Cells on Graphene Oxide/poly-L-Lysine Composite Films, J. Mater. Chem. B 2 (2014) 5461–5467, https://doi.org/10.1039/c4tb00856a.
[60] Z. Tian, L. Huang, X. Pei, J. Chen, T. Wang, T. Yang, H. Qin, L. Sui, J. Wang, Electrochemical Synthesis of Three-Dimensional Porous Reduced Graphene Oxide Film: Preparation and In Vitro Osteogenic Activity Evaluation, Colloids Surfaces B Biointerfaces 155 (2017) 150–158, https://doi.org/10.1016/j.colsurfb.2017.04.012.
[61] Y. Zhang, D. Zhai, M. Xu, Q. Yao, J. Chang, C. Wu, 3D-Printed Bioceramic Scaffolds with a Fe3O4/graphene Oxide Nanocomposite Interface for Hyperthermia Therapy of Bone Tumor Cells, J. Mater. Chem. B 4 (2016) 2874–2886, https://doi.org/10.1039/c6tb00390g.